Polar Ultraviolet Imager observation of auroral breakup

Kan Liou[1]

Received 19 April 2010; revised 10 September 2010; accepted 15 September 2010; published 9 December 2010.

[1] The NASA's Polar satellite completed its mission in March 2008. During its 12 year operation, the Ultraviolet Imager (UVI) on-board Polar acquired a large number of auroral images in FUV bands with unprecedented spatial and temporal resolutions. The purpose of this brief report is to provide a list of auroral substorm onset identified with UVI to the community for full use. A total of 2003 auroral substorm onsets are identified in the Northern Hemisphere between 1996 and 2000 and 536 onsets in Southern Hemisphere in 2007. Distributions of the onset locations are near Gaussian, with a population mean of 65.9° (standard deviation σ = 2.2°) in magnetic latitude (MLat) and 22.6 (σ = 1.1) in magnetic local time (MLT) for the northern hemispheric events and 68.0° (σ = 2.3°) in MLat and 22.6 (σ = 1.1) in MLT for the southern hemispheric events. A comparison with previously published IMAGE onset results suggests that substorms occur more frequently and intensely in the descending than in the ascending phase of solar cycle. The list of onset events includes the onset times and locations, and is provided as a supplement.

Citation: Liou, K. (2010), Polar Ultraviolet Imager observation of auroral breakup, *J. Geophys. Res.*, *115*, A12219, doi:10.1029/2010JA015578.

1. Introduction

[2] The auroral substorm is a visual manifestation of the magnetospheric substorm that involves an explosive dissipation of electromagnetic energy from the magnetosphere to the Earth's upper atmosphere. As first described by *Akasofu* [1964], the concept of auroral substorm consists of a sequence of changes in auroral displays repeatably seen in the premidnight sector. The sequence begins as quiet, parallel auroral arcs moving equatorward, which is later known as the growth phase of substorm [*McPherron*, 1972]. At a certain point, a sudden brightening of the most equatorward existing arcs or a new arc, known as onset or "auroral breakup," to an explosive increase in auroral luminosity and area (the expansion phase), and then from a very disturbed auroral state to the original quiet time at a much slower pace (the recovery phase).

[3] Auroral breakup defines the conjugate foot point of magnetospheric substorm onset region in the ionosphere. Information about the location where the magnetospheric substorm is first initiated is important to substorm research. For example, direct observations of signatures of reconnection from Geotail suggest that the typical near-Earth neutral line at substorm onset was located ~20 R_E tailward of the Earth [*Baumjohann et al.*, 1990; *Miyashita et al.*, 2003]. On the other hand, in situ measurements of cross-tail current disruption and its associated magnetic field line dipolarization suggest that substorm expansion phase onset starts in the near-Earth plasma sheet (4–10 R_E) [e.g., *Jacquey et al.*, 1991; *Lui et al.*, 1991]. Timing analysis of various substorm onset identifiers suggest that substorms are initiated earthward of ~15 R_E [*Liou et al.*, 2000, 2001a, 2002]. Some careful studies using global FUV images map the arcs even closer to the Earth, ~9 R_E during relative magnetic quiet times and ~5–7 R_E during magnetic active times [*Frank and Sigwarth*, 2000]. Therefore, tail reconnection, which occurs typically several Earth radii tailward of the observed onset signatures, cannot be the direct cause of substorm expansion onset. To amend the deficiency of the near-Earth neutral line model, some researchers proposed that braking of high-speed earthward plasma flows, which are often observed in the plasma sheet near midnight meridian during high-*AE* values [*Baumjohann et al.*, 1990], can set up the substorm wedge current system in the near-Earth tail regions [*Shiokawa et al.*, 1997; *Birn et al.*, 1999].

[4] Several other substorm models exist in addition to the one mentioned above. These models include the cross-field current instability [*Lui et al.*, 1991], ballooning mode instability [*Roux et al.*, 1991], magnetosphere-ionosphere coupling [*Kan et al.*, 1988], boundary layer dynamics model [*Rostoker and Eastman*, 1987], thermal catastrophe model [*Goertz and Smith*, 1989], and convection reduction model [*Lyons*, 1995]. Given a precise onset time and location, these onset models can be critically examined with plasma and field parameters measured prior to and at the onset. This can be done either by case studies with conjunction events or statistical studies that give the average values for the required parameters. The latter approach has been employed by a number of researchers [e.g., *Lui et al.*, 1998; *Nakamura et al.*, 2001; *Miyashita et al.*, 2003; *Ieda et al.*, 2008, and references therein].

[1]Johns Hopkins University Applied Physics Laboratory, Laurel, Maryland, USA.

0148-0227/10/2010JA015578

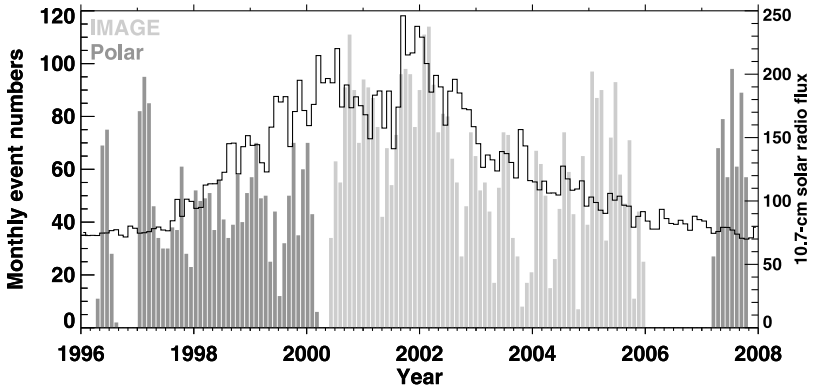

Figure 1. Monthly auroral substorm onset events identified with FUV auroral images acquired by Polar (dark gray) and IMAGE (light gray) satellites. The 10.7 cm solar radio flux is overlapped (black histogram).

[5] The purpose of this paper is to report a large number of auroral breakup events identified with satellite auroral images. These breakup events will be tagged with time and geographic and geomagnetic coordinates of the onset location to allow full use by interested researchers. Similar work has been performed by *Frey et al.* [2004] and *Frey and Mende* [2006], who published a combined list of 4193 auroral breakup events identified with global auroral images acquired by FUV imagers [*Mende et al.*, 2000] on board the IMAGE satellite. Their onset list covers the entire mission of the IMAGE satellite during periods around the maximum and the descending phase of solar cycle 23 (2000–2006). Monthly distributions of the events are plotted in light gray in Figure 1. The large number of onset events have been used frequently to study, for instance, magnetospheric dynamics [e.g., *Kim et al.*, 2008, *Boakes et al.*, 2009] and ionospheric flows [e.g., *Bristow*, 2009; *Liang et al.*, 2006] during substorms. Auroral image data used in this work will be based on the Polar satellite. Auroral images taken from Polar occurred mostly during the minimum and early ascending phase of solar cycle 23 (1996–1999 and 2007), when the inclination of Polar was large enough. Therefore, the present work result will complement the IMAGE result to form a near-complete database of auroral breakup for the entire solar cycle 23, allowing studies of solar cycle variations of substorm-associated near-space phenomena.

2. Instrumentation

[6] The ultraviolet imager (UVI) [*Torr et al.*, 1995] is a 2-D snapshot type of camera on-board the Polar satellite, which was launched on 24 February 1996 and ended in April 2008. The UVI optical sensor operated in four-filter band passes: two atomic oxygen lines centered at 130.4 and 135.6 nm and two molecular nitrogen Lyman-Birge-Hopfield bands centered at ~150 nm (LBHs) and ~170 nm (LBHl). With a circular field of view of 8°, typical spatial resolution provided by the Polar UVI is about 30–40 km at an assumed 120 km emission height for images taken near the apogee of ~9 R_E. The wobble of the satellite degrades the resolution significantly in a fixed direction. The wobble period is ~6 s, which is much shorter than the 36.8 s integration time, and is not likely to introduce artificial growth of the aurora between images, which otherwise makes onset identification difficult. The Polar UVI has acquired more than a decade's worth of Earth disk images during the entire Polar mission. Because the Polar orbital plane slowly drifted southward, the best viewing period for the northern oval is before the year of 2000. Considerably fewer auroral images were available after 2000 because of large viewing angles and most of the bandwidth for data down-link was appropriated to other instruments. In 2007 and 2008, Polar apogee was in the Antarctic region, and image data down-link was resumed to support the THEMIS mission.

3. Determination of Auroral Breakup

[7] In this study, auroral breakups are visually identified from Polar UVI images on the basis of the classical auroral substorm scheme [*Akasofu*, 1964] with a small modification. This is because determining auroral substorm onsets with global auroral images is slightly different from that with ground-based all-sky images. All-sky imager provides much better spatial resolution than current global auroral imager and can distinguish auroral arcs that global auroral imager cannot. Furthermore, all-sky imager has better sensitivity and temporal resolution than global auroral imager. As a result, fine structure auroral dynamics prior to and associated with onset can be clearly identified with the all-sky imager but not with the global imager. However, past experience indicates that substorm onset determined with Polar UVI images can be as reliable as those determined with all-sky images to within ~1 min. On the other hand, there are advantages in using global auroral images to identify auroral breakups. The much wider field of view provided by global auroral imagers can unambiguously determine substorm events and their onset locations, whereas the much smaller field of view of all-sky imagers cannot. Inexperienced workers can sometimes misidentify auroral surge as an auroral breakup. Moreover, with FUV filters, Polar UVI can image the auroral oval in full sunlight, whereas all-sky cameras can only work during darkness.

[8] We first carefully examine a sequence of raw images from the UVI database. Once a substorm event, which consists of a sudden brightening of the aurora followed by a subsequent growing in the auroral intensity and region, is

identified, the images are calibrated and reformatted in the altitude-adjusted corrected geomagnetic (AACGM) coordinate system (formerly PACE Geomagnetic Coordinates [*Baker and Wing*, 1989]). Normally, we examine processed auroral images for a time interval of ~10 min before and after a tentative onset (sudden brightening). This basically imposes a ~10 min minimum duration for the auroral intensification. A thorough inspection of the substorm process is performed to make sure that the onset is followed by a continuing poleward and zonal expansion of the substorm bulge (expansion phase). We do not require the poleward expansion to be over the poleward boundary of the oval, however. This is because the nightside oval is often not visible around onset. In general, a few degrees poleward expansion and 1–2 h magnetic local time widening are the minimal requirement. This is done by tracing substorm features back in time and finding the first brightening (auroral breakup) in the oval. Once the onset image is determined, we use the so-called "region growing" image processing technique to determine bright pixels associated with the onset. After the onset pixels on the image are determined, we calculate the centroid location of the auroral onset in terms of magnetic latitude and local time weighted by intensity (see *Liou et al.* [2006] for details). Because the determination of the onset location is pixel based, there is an intrinsic uncertainty of ~±20 km at nadir. In reality, the total observation accuracy is probably close to ~1 degree in latitude. Of further note, we ignore events if auroral intensifications, which frequently occur minutes after onset, take place at the poleward edge of the auroral surge. On the other hand, events with intensifications initiated at a lower latitude equatorward of the surge head will be counted as a new breakup. On a rare occasion, two distinct onsets can occur simultaneously at different locations. When that happens, one of the onsets usually grows faster and takes over the other. We consider the dominant one as the true onset.

4. Results and Discussion

4.1. Chronological Distributions of Auroral Onsets

[9] The surveyed data set covers periods from March 1996 to February 2000 for the Northern Hemisphere and the entire year of 2007 for the Southern Hemisphere.[1] There are a total of 2003 onsets in the Northern Hemisphere and 536 onsets in the Southern Hemisphere, giving a total of 2539 identified onsets. The monthly distribution of identified auroral onsets is plotted chronologically in dark gray in Figure 1. Obviously, the onset list does not include all substorms that occurred within the surveyed periods as the Polar is an orbital satellite and cannot monitor the auroral ovals 24 h each day. Furthermore, auroral activations without "clear" onset are excluded from the list. A clear onset should consist of a recognizable sudden brightening of localized aurora followed by a subsequent growing in the auroral intensity and region as discussed in Section 3. Some auroral activations do not show such a time sequence of development in UVI images. For example, during storm times, enhancements of aurora in a large part of or the entire oval can occur within one or two image frames, making identification of onset location impossible. In general, the onset list is composed of auroral breakup with identifiable onset times and locations, which require continuous data coverage around (~±10 min) the onset time and the onset location. The uncertainty of the onset timing is greater when multifilter images (which rotate in sequence) are used; however, this uncertainty is greatly reduced to the UVI frame rate (37 s) after December 1996 because the LBH-long filter was used primarily until the end of the Polar mission. We have also provided animated auroral substorm movies in mpeg format for selected events (from 4 December 1996 to 31 May 1997) online (available at http://sd-www.jhuapl..edu/Auroral). The onset list, provided as a supplement, includes the date of the event, time of the first brightening image and time of the one before, and the latitude and local time in AACGM geomagnetic coordinates [*Baker and Wing*, 1989] and geographic coordinates.

[10] Auroral substorm onset events identified with Polar data in this study span the early ascending phase (1996–2000) and the end of (2007) solar cycle 23, whereas those identified with IMAGE data [*Frey et al.*, 2004; *Frey and Mende*, 2006] cover part of the late ascending phase and most of the descending phase of solar cycle 23 (2000–2006). Therefore, except for the second half of 1996 and the entire year of 2006 as well as a small data gap in early 2000, combination of the two provide a complete set of auroral breakup events for the solar cycle 23. As shown in Figure 1, it is immediately apparent that there are more monthly events from IMAGE than from Polar. For instance, the largest event number occurs in 2002, coinciding with the peak of 10.7 cm solar radio flux (plotted as a histogram in black in Figure 1). At first glance, this is consistent with the general notion that most intense magnetic and auroral activity occurs during solar maximum. However, the correlation coefficient between the onset number and the F107 index is small (r = 0.30). This is because the onset events also show increases in solar minimum years (e.g., 1996–1997, 2005, and 2007).

[11] It is important to note that one must be very careful when interpreting the result shown in Figure 1. First, these onset numbers have not been normalized to the observation time for both Polar and IMAGE. Substantial reductions in the onset events are expected for periods of short observation time. For example, the data gap in the second half of 1996, when the first UVI imager started showing signs of malfunction, and between 24 March and 13 April 2001, when IMAGE FUV was not operating [*Frey et al.*, 2004]. Second, there is a systematic decrease in the measurement time. This is because the apogee of both Polar and IMAGE orbits changes in time such that it moves slowly from high latitudes to low latitudes, resulting in reducing imaging time per orbits. This occurred after 1999 for Polar and 2002–2004 for IMAGE. For Polar, the effect is more significant because of the smaller field of view of the UVI. The increase in the onset number in 2005 is probably because IMAGE apogee had moved to the high latitude of the Southern Hemisphere. On the other hand, we suspect that the increase may be associated with the increase in the number of high-speed streams (HSSs) in the solar wind, which maximizes in minimum and declining phase years [*Bame et al.*, 1976]. In HSS, strong perpendicular Alfvénic fluctuations are com-

[1] Auxiliary materials are available at ftp://ftp.agu.org/apend/ja/2010ja015578.

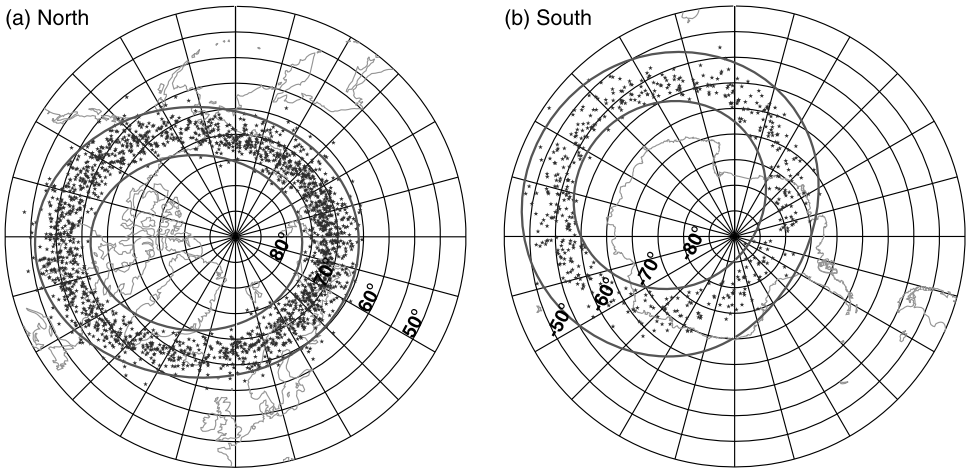

Figure 2. Geographic locations of auroral substorm onset (stars) identified from Polar UVI images for (a) Northern Hemisphere (2003 events) and (b) Southern Hemisphere (536 events). Contours of 62° and 72° MLat for Northern Hemisphere and −62° and −72° for Southern Hemisphere are plotted in bold gray, and continents are plotted in light gray.

monly present [*Belcher and Davis*, 1971], which provide large-amplitude north-south magnetic fields and cause significant intermittent geomagnetic [e.g., *Tsurutani et al.*, 1995] and auroral disturbances [e.g., *Liou*, 2006]. We suspect that a similar increase in the onset numbers in the solar minimum years (1996–1997, and 2007) observed by Polar could also be due to the same cause. Work that conducts statistical studies of the relationship between onsets and Alfvénic waves in HSSs is required to confirm this thought.

[12] Of further note, the methodology adopted by IMAGE is slightly different from that used in this study for Polar. The major difference is that IMAGE requires that the aurora has to expand to the poleward boundary of the oval and spread azimuthally in local time for at least 20 min and there must be at least 30 min of separation between events. In this study we limit these times to ~10 min. Also, we do not require an auroral bulge expanding poleward of the oval poleward boundary. These imply that more weak events are included in Polar than in IMAGE onset list. In other words, had we adopted the same criteria used by *Frey et al.* [2004], we would have found less onset events. Nonetheless, even with these caveats, it is reasonable to suggest that substorm activity is more frequent and intense in the descending phase of a solar cycle.

4.2. Spatial Distributions of Auroral Onsets

[13] Figure 2 shows spatial distributions of the identified auroral onset locations in geographic coordinates for the Northern Hemisphere (Figure 2a) and Southern Hemisphere (Figure 2b). These onset events cover an oval-shaped annular region of ~10° width in latitude, with ~95% of events located between 62° and 72° MLat and ~68% of events located between 65° and 70° MLat. Although the total number of events for the Southern Hemisphere is significantly less than that for the Northern Hemisphere, the onsets are approximately distributed evenly in a circular region.

[14] Figure 3a shows distributions of the onset locations in AACGM magnetic latitude–magnetic local time (MLat-MLT) format. Onsets that occurred in both hemispheres are combined and the result is presented in the northern hemispheric view. Figures 3b and 3c show histograms of the onset latitude and local time, respectively. The histograms are nonlinear least squares fitted to a Gaussian function. The fit gives a mean magnetic latitude $\mu = 66.1°$ (variance $\sigma^2 = 4.85$) and a mean magnetic local time $\mu = 22.6$ ($\sigma^2 = 1.22$). The Gaussian is a well-chosen probability function because the χ^2 test of goodness-of-fit suggests that both Gaussian curve fits are acceptable at or better than the 0.05 significant level ($\chi^2 = 1.25 < \chi^2_{\text{cutoff}}(\alpha = 0.05, \text{n} = 13) = 22.4$ for MLat and $\chi^2 = 1.10 < \chi^2_{\text{cutoff}}(\alpha = 0.05, \text{n} = 14) = 23.7$ for MLT). Based on the sigma rules, the majority (~68%) of onsets occur in between 63.9°–68.3° in MLat and 21.5–23.7 in MLT and slightly more than 95% of onsets occur within the range 61.7°–70.5° in MLat and 20.4–24.8 in MLT.

[15] To compare directly with previous results from IMAGE (listed in Table 1), we compute the sample mean of onset location, which results in 66.30° (standard deviation of the sample $s_N = 2.41$) MLat and 22.88 ($s_N = 1.12$) MLT. *Frey et al.* [2004] identified 2437 auroral substorm onsets based on auroral images acquired by FUV cameras [*Mende et al.*, 2000] on-board the IMAGE satellite and found that those substorms occurred on average at 66.1° MLat and 23.0 MLT (more precisely 66.06° ($s_N = 2.86$) MLat and 22.95 ($s_N = 1.35$) MLT, recalculated from their published onset events). Assuming onset locations from both observations are normally distributed, the normal deviate test rejects the null hypothesis that the onsets observed separately by Polar and IMAGE have the same mean locations if one adopts the 0.05 significant level. A lower average onset latitude in the IMAGE result is consistent with the fact that IMAGE data were acquired during higher solar magnetic activity, and therefore higher geomagnetic activity, than Polar data. A quantitative answer will require more detailed analysis of the solar wind/IMF conditions during the onset events. Unfortunately this is outside the scope of the present study. The sample means of onset location from other observations, such as DE-1

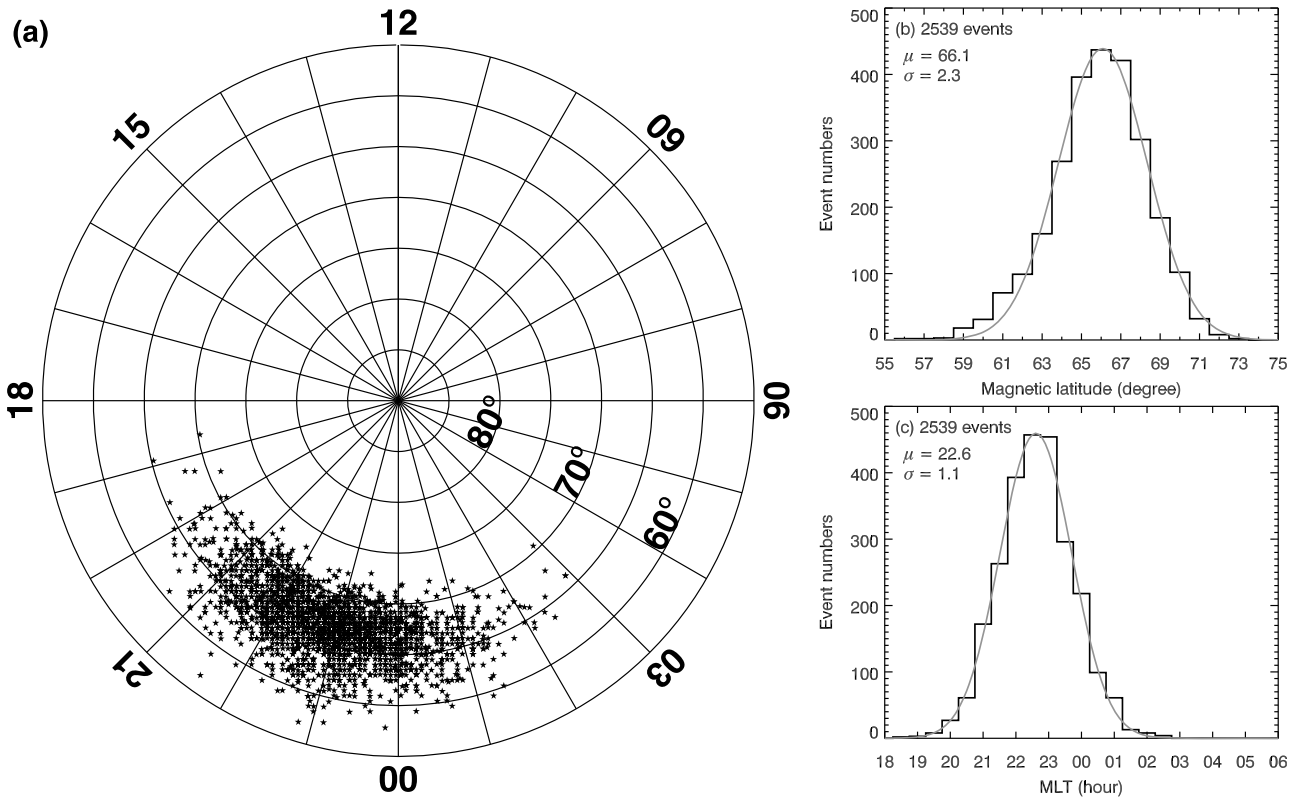

Figure 3. (a) Distributions of 2539 auroral substorm onset locations in AACGM magnetic local time-magnetic latitude coordinates [*Baker and Wing*, 1989]; on the right are histograms of the onset (b) magnetic latitude with 1° MLat increments and (c) magnetic local time in half-hour bins. Smooth (gray) lines superimposed in Figures 3b and 3c are a Gaussian function least squares fitted to the histograms. The mean (μ) and standard deviation (σ) are indicated.

[*Craven and Frank*, 1991] and Viking [*Henderson and Murphree*, 1995], are also given in Table 1.

4.3. Comparison of Northern and Southern Hemispheric Onset Location

[16] Reports based on observations of auroral substorm onsets in the Southern Hemisphere are rare. It is generally believed that substorms are initiated in the plasma sheet closed field lines; as a consequence, substorm onset must be conjugate. A few case studies have shown that there is an azimuthal displacement of onset locations between the two hemispheres under conditions of a large IMF B_y component [*Østgaard et al.*, 2004]. However, there is no report about the statistical onset location in Southern Hemisphere. Here we separate the 2539 identified onset events by hemispheres and analyze their statistical onset locations. Figure 4 shows normalized histograms of magnetic onset latitudes (Figure 4, top) and local times (Figure 4, bottom) for the Northern Hemispheric (Figure 4, left) and the Southern Hemispheric (Figure 4, right) events. A suitably normalized Gaussian distribution function is superimposed in each histogram. The χ^2 goodness-of-fit test suggests that these fits are at or better than the 0.05 significance level, indicating that the Gaussian is a well-chosen probability function. The population mean of the onset location is 65.9° (variance $\sigma^2 = 4.85$) in MLat and 22.6 ($\sigma^2 = 1.22$) in MLT for the Northern Hemisphere and 68.0° ($\sigma^2 = 5.24$) in MLat and 22.6 ($\sigma^2 = 1.14$) in MLT for the Southern Hemisphere. According to the normal deviate test, the assumption of equal means would produce a deviation as large as or larger than that observed 37% in MLat and 0% in MLT. This means that differences between the mean northern and southern onset local time are negligible, whereas differences in the mean southern and northern onset latitude (2.1°) are statistically significant. The

Table 1. Arithmetic Mean Values of Auroral Onset Location From Previous and Present Statistical Studies

Satellite	Samples	MLT (hour)	MLat (deg)	References
DE-1	68	22.8	?	*Craven and Frank* [1991]
Viking	133	22.8	65.8°	*Henderson and Murphree* [1995]
Polar (first year)	648	22.7	66.6°	*Liou et al.* [2001b]
IMAGE	2437	22.95 ± 0.02	66.06° ± 0.03°	*Frey et al.* [2004]
Polar	2539	22.88 ± 0.02	66.30° ± 0.05°	Present paper

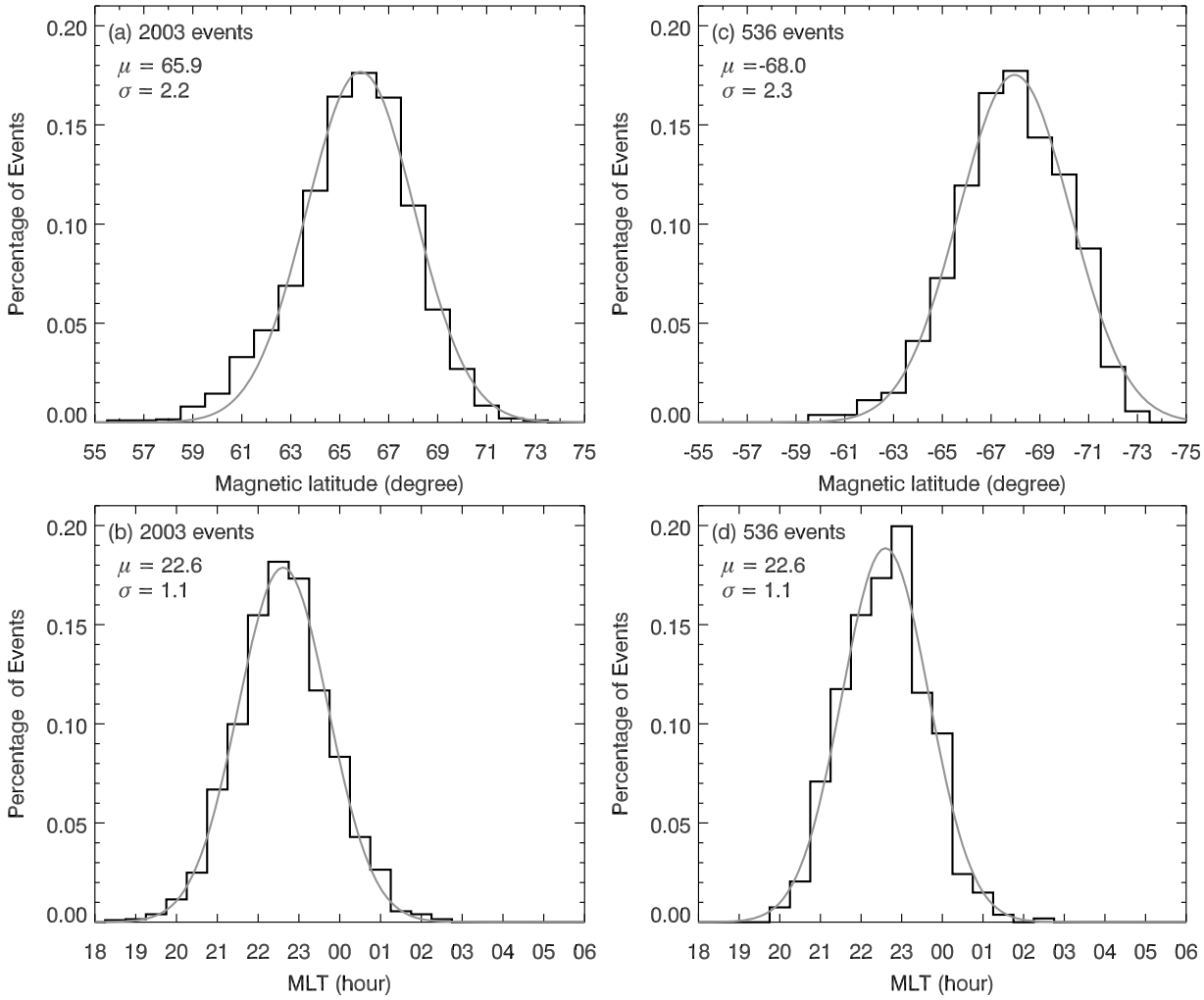

Figure 4. Histograms of auroral substorm onset locations in (top) magnetic latitude and (bottom) local time for (a and b) Northern and (c and d) Southern Hemisphere. A suitably normalized Gaussian curve is superimposed. The format is the same as Figures 3b and 3c.

difference is probably due to different solar wind conditions. It is well known that the location of auroral breakups moves to lower latitudes for more negative IMF B_z and to higher latitudes for less negative IMF B_z. To test this hypothesis, we calculate averages of the 60 min average of IMF B_z immediately prior to onset, which yields −1.3 (s_N = 2.5) nT for the northern hemispheric events and −0.1 (s_N = 1.6) nT for the southern hemispheric events. One can easily show, with a standard deviate test, that the difference in IMF B_z values is significant. On the basis of previous [*Liou et al.*, 2001b] and present observations, the location of auroral breakup moves ~0.6°–0.7° equatorward in MLat for every 1 nT decrease in hourly averages of IMF B_z component. Therefore IMF B_z can only explain ~0.8° difference. With a difference of the mean of onset location of 2.1° in MLat and an observation accuracy of ~1°, it suggests that other parameters may be involved. A detailed analysis of all possible solar wind drivers is necessary and will be performed in a future study.

[17] Finally, it is worth pointing out that differences in the standard deviations of onset locations between northern and southern onsets are small. It may suggest that the underlying physical processes associated with substorms are the same for the two hemispheres. This is not unexpected because both northern and southern onsets share the same origin.

5. Summary

[18] A list of 2539 auroral substorm events are identified with Polar UVI image data acquired in the Northern Hemisphere between 1996 and 2000 and in the Southern Hemisphere in 2007. The onset list is included as a supplement to this article. It can also be obtained from a designated APL website (available at http://sd-www.jhuapl.edu/Auroral). We expect that the published onset list will be useful in several space physics disciplines. The onset list complements another large onset list published by *Frey et al.* [2004], which covers the years around the maximum and the descending phase of solar cycle 23, whereas onset events observed by Polar UVI cover the minimum and the ascending phase of solar cycle 23.

[19] Comparing with previously reported results based on different satellite image data acquired during different times, it is found that there are statistical differences in the average onset locations, though the differences are generally small. There is also evidence suggesting that substorms occur more frequently and probably more intensely in the descending phase of solar cycle.

[20] **Acknowledgments.** We acknowledge that G. Parks was the PI of Polar UVI, which was originally built by M. Torr. We acknowledge the use of OMNI magnetic field data supplied by NSSDC and the use of F107 solar index supplied by NOAA Geophysical Data Center. This study was supported by NSF grant ATM-0703414 and NASA grants NNX08AN32G and NNX06AB88G to the Johns Hopkins University Applied Physics Laboratory.

[21] Robert Lysak thanks the reviewers for their assistance in evaluating this paper.

References

Akasofu, S.-I. (1964), The development of the auroral substorm, *Planet. Space Sci.*, *12*(4), 273–282, doi:10.1016/0032-0633(64)90151-5.

Baker, K., and S. Wing (1989), A new magnetic coordinate system for conjugate studies at high latitudes, *J. Geophys. Res.*, *94*(A7), 9139–9143, doi:10.1029/JA094iA07p09139.

Bame, S. J., J. R. Asbridge, W. C. Feldman, and J. T. Gosling (1976), Solar cycle evolution of high speed solar wind streams, *Astrophys. J.*, *207*, 977–980, doi:10.1086/154566.

Baumjohann, W., G. Paschmann, and H. Lühr (1990), Characteristics of high-speed ion flows in the plasma sheet, *J. Geophys. Res.*, *95*(A4), 3801–3809, doi:10.1029/JA095iA04p03801.

Belcher, D., and L. Davis (1971), Large-amplitude Alfvén waves in the interplanetary medium, *J. Geophys. Res.*, *76*, 3534–3563, doi:10.1029/JA076i016p03534.

Birn, J., M. Hesse, G. Haerendel, W. Baumjohann, and K. Shiokawa (1999), Flow braking and the substorm current wedge, *J. Geophys. Res.*, *104*(A9), 19,895–19,903, doi:10.1029/1999JA900173.

Boakes, P. D., S. E. Milan, G. A. Abel, M. P. Freeman, G. Chisham, and B. Hubert (2009), A statistical study of the open magnetic flux content of the magnetosphere at the time of substorm onset, *Geophys. Res. Lett.*, *36*, L04105, doi:10.1029/2008GL037059.

Bristow, W. A. (2009), Relationship between substorm onset locations and nightside convection pattern features, *J. Geophys. Res.*, *114*, A12202, doi:10.1029/2009JA014576.

Craven, J. D., and L. A. Frank (1991), Diagnosis of auroral dynamics using global auroral imaging with emphasis on large-scale evolution, in *Auroral Physics*, edited by C.-I. Meng, M. J. Rycroft, and L. A. Frank, pp. 273–297, Cambridge Univ. Press, New York.

Frank, L. A., and J. B. Sigwarth (2000), Findings concerning the positions of substorm onsets with auroral images from the Polar spacecraft, *J. Geophys. Res.*, *105*(A6), 12,747–12,761, doi:10.1029/1999JA000356.

Frey, H. U., and S. B. Mende (2006), Substorm onsets as observed by IMAGE-FUV, in *Proceedings of Eighth International Substorm Conference*, edited by M. Syrjäsuo and E. Donovan, pp. 71–76, Univ. of Calgary, Banff Centre, Canada, 27–31 March.

Frey, H. U., S. B. Mende, V. Angelopoulos, and E. F. Donovan (2004), Substorm onset observations by IMAGE-FUV, *J. Geophys. Res.*, *109*, A10304, doi:10.1029/2004JA010607.

Goertz, C. K., and R. A. Smith (1989), The thermal catastrophe model for substorms, *J. Geophys. Res.*, *94*(A6), 6581–6596, doi:10.1029/JA094iA06p06581.

Henderson, M., and J. Murphree (1995), Comparison of Viking onset locations with the predictions of the thermal catastrophe model, *J. Geophys. Res.*, *100*(A11), 21,857–21,872, doi:10.1029/95JA00416.

Ieda, A., et al. (2008), Longitudinal association between magnetotail reconnection and auroral breakup based on Geotail and Polar observations, *J. Geophys. Res.*, *113*, A08207, doi:10.1029/2008JA013127.

Jacquey, C., J. A. Sauvaud, and J. Dandouras (1991), Location and propagation of the magnetotail current disruption during substorm expansion: Analysis and simulation of an ISEE multi-onset event, *Geophys. Res. Lett.*, *18*(3), 389–392, doi:10.1029/90GL02789.

Kan, J. R., L. Zhu, and S.-I. Akasofu (1988), A theory of substorms: Onsets and subsidence, *J. Geophys. Res.*, *93*(A6), 5624–5640, doi:10.1029/JA093iA06p05624.

Kim, H.-J., D.-Y. Lee, and L. R. Lyons (2008), Are repetitive particle injections during high-speed solar wind streams classic substorms?, *J. Geophys. Res.*, *113*, A08205, doi:10.1029/2007JA012847.

Liang, J., G. J. Sofko, and H. U. Frey (2006), Postmidnight convection dynamics during substorm expansion phase, *J. Geophys. Res.*, *111*, A04205, doi:10.1029/2005JA011483.

Liou, K. (2006), Global auroral responses to interplanetary media with emphasis on solar wind dynamic pressure enhancements, in *Chapman Conference on Recurrent Magnetic Storms: Corotating Solar Wind Streams*, *Geophys. Monogr. Ser.*, vol. 167, edited by B. T. Tsurutani et al., pp. 197–212, AGU, Washington, D. C.

Liou, K., C.-I. Meng, P. Newell, K. Takahashi, S.-I. Ohtani, A. Lui, M. Brittnacher, and G. Parks (2000), Evaluation of low-latitude Pi2 pulsations as indicators of substorm onset using Polar ultraviolet imagery, *J. Geophys. Res.*, *105*(A2), 2495–2505, doi:10.1029/1999JA900416.

Liou, K., C.-I. Meng, P. Newell, A. Lui, G. Reeves, and R. Belian (2001a), Particle injections with auroral expansions, *J. Geophys. Res.*, *106*(A4), 5873–5881, doi:10.1029/2000JA003003.

Liou, K., P. T. Newell, D. G. Sibeck, C.-I. Meng, M. Brittnacher, and G. Parks (2001b), Observation of IMF and seasonal effects in the location of auroral substorm onset, *J. Geophys. Res.*, *106*(A4), 5799–5810, doi:10.1029/2000JA003001.

Liou, K., C.-I. Meng, A. T. Y. Lui, P. T. Newell, and S. Wing (2002), Magnetic dipolarization with substorm expansion onset, *J. Geophys. Res.*, *107*(A7), 1131, doi:10.1029/2001JA000179.

Liou, K., C.-I. Meng, and C.-C. Wu (2006), On the interplanetary magnetic field B_y control of the substorm bulge expansion, *J. Geophys. Res.*, *111*, A09312, doi:10.1029/2005JA011556.

Lui, A., C.-L. Chang, A. Mankofsky, H.-K. Wong, and D. Winske (1991), A cross-field current instability for substorm expansions, *J. Geophys. Res.*, *96*(A7), 11,389–11,401, doi:10.1029/91JA00892.

Lui, A. T. Y., K. Liou, P. T. Newell, C.-I. Meng, S.-I. Ohtani, T. Ogino, S. Kokubun, M. J. Brittnacher, and G. K. Parks (1998), Plasma and magnetic flux transport associated with auroral breakups, *Geophys. Res. Lett.*, *25*(21), 4059–4062, doi:10.1029/1998GL900022.

Lyons, L. (1995), A new theory for magnetospheric substorms, *J. Geophys. Res.*, *100*(A10), 19,069–19,081, doi:10.1029/95JA01344.

McPherron, R. L. (1972), Substorm related changes in the geomagnetic tail: The growth phase, *Planet. Space Sci.*, *20*(9), 1521–1539, doi:10.1016/0032-0633(72)90054-2.

Mende, S. B., et al. (2000), Far ultraviolet imaging from the IMAGE spacecraft, *Space Sci. Rev.*, *91*(1/2), 271–285, doi:10.1023/A:1005227915363.

Miyashita, Y., S. Machida, K. Liou, T. Mukai, Y. Saito, H. Hayakawa, C.-I. Meng, and G. K. Parks (2003), Evolution of the magnetotail associated with substorm auroral breakups, *J. Geophys. Res.*, *108*(A9), 1353, doi:10.1029/2003JA009939.

Nakamura, R., W. Baumjohann, M. Brittnacher, V. Sergeev, M. Kubyshkina, T. Mukai, and K. Liou (2001), Flow bursts and auroral activations: Onset timing and foot point location, *J. Geophys. Res.*, *106*(A6), 10,777–10,789, doi:10.1029/2000JA000249.

Østgaard, N., S. B. Mende, H. U. Frey, T. J. Immel, L. A. Frank, J. B. Sigwarth, and T. J. Stubbs (2004), Interplanetary magnetic field control of the location of substorm onset and auroral features in the conjugate hemispheres, *J. Geophys. Res.*, *109*, A07204, doi:10.1029/2003JA010370.

Rostoker, G., and T. Eastman (1987), A boundary layer model for magnetospheric substorms, *J. Geophys. Res.*, *92*(A11), 12,187–12,201, doi:10.1029/JA092iA11p12187.

Roux, A., S. Perraut, P. Robert, A. Morane, A. Pedersen, A. Korth, G. Kremser, B. Aparicio, D. Rodgers, and R. Pellinen (1991), Plasma sheet instability related to the westward traveling surge, *J. Geophys. Res.*, *96*(A10), 17,697–17,714, doi:10.1029/91JA01106.

Shiokawa, K., W. Baumjohann, and G. Haerendel (1997), Braking of high-speed flows in the near-Earth tail, *Geophys. Res. Lett.*, *24*(10), 1179–1182, doi:10.1029/97GL01062.

Torr, M. R., et al. (1995), A far ultraviolet imager for the international solar-terrestrial physics mission, *Space Sci. Rev.*, *71*(1–4), 329–383, doi:10.1007/BF00751335.

Tsurutani, B. T., W. D. Gonzalez, A. L. C. Gonzalez, F. Tang, J. K. Arballo, and M. Okada (1995), Interplanetary origin of geomagnetic activity in the declining phase of the solar cycle, *J. Geophys. Res.*, *100*(A11), 21,717–21,733, doi:10.1029/95JA01476.

K. Liou, Johns Hopkins University Applied Physics Laboratory, 11100 Johns Hopkins Rd., Laurel, MD 20723, USA. (kan.liou@jhuapl.edu)